Nonlinear extended wave-equation imaging by image-domain seismic interferometry

Ivan Vasconcelos[1], Paul Sava[2] & Huub Douma[1]
[1] *ION Geophysical, GXT Imaging Solutions.*
[2] *Center for Wave Phenomena, Colorado School of Mines*

ABSTRACT
Wave-equation, finite-frequency imaging and inversion still faces considerable challenges in addressing the inversion of highly complex velocity models as well as in dealing with nonlinear imaging (e.g., migration of multiples, amplitude-preserving migration). Extended images (EI's), as we present here, are particularly important for designing image-domain objective functions aimed at addressing standing issues in seismic imaging such as two-way migration velocity inversion or imaging/inversion using multiples. Using general two- and one-way representations for scattered wavefields, we describe and analyze EI's obtained in wave-equation imaging. The presented formulation explicitly connects the wavefield correlations done in seismic imaging with the theory and practice of seismic interferometry. We define extended images as locally scattered fields reconstructed by model-dependent, image-domain interferometry. Because we use the same two- and one-way scattering representations that are used for seismic interferometry, the reciprocity-based EI's can in principle account for all possible nonlinear effects in the imaging process, i.e., migration of multiples, amplitude corrections, etc. In that case, the practice of two-way imaging departs considerably from that of the one-way approach. Here we elaborate on the differences between these approaches in the context of nonlinear imaging, describing these differences both in the wavefield extrapolation steps as well as in imposing the extended imaging conditions. When invoking single-scattering and ignoring amplitude effects in generating EI's, the one- and two-way approaches become essentially the same as those employed in today's migration practice, with the straightforward addition of space- and time-lags in the correlation-based imaging condition. Our formal description of the EI's and the insight that they are scattered fields in the image-domain may be useful in further development of imaging and inversion methods: either in the context of linear, migration-based velocity inversion, or in more sophisticated image-domain nonlinear inverse scattering approaches.

Key words: Inverse scattering, wave equation, imaging, interferometry.

1 INTRODUCTION

Seismic imaging and model estimation still present daunting challenges to the geophysical community when it comes to dealing with areas of high structural complexity or in making use of nonlinear scattering present in the data (in the form of e.g., multiples or amplitude effects). One avenue to address these challenges are the so-called full-waveform inversion methods (e.g., Tarantola, 1984; Pratt, 1999; Sirgue and Pratt, 2004; Plessix, 2006; Tape et al., 2009; Zhu et al., 2009). These methods operate by finding models that best fit the recorded data, and although in principle they are well suited to handle nonlinear scattering effects in the data, waveform inversion methods are notoriously ill-posed in terms of their sensitivity to the choice of starting models. An al-

ternative to deal with the ill-posedness of data-domain nonlinear inversions such as waveform inversion or inverse scattering approaches (e.g., Rose et al., 1985; Budreck and Rose, 1990; Weglein et al., 2003) is to set up the inverse problem in the subsurface image domain (e.g., de Hoop et al., 2006; Symes 2008, 2009). These approaches have demonstrated their potential for linear, wave-equation migration-based velocity inversion (e.g., Chauris, 2000; Mulder and Ten Kroode, 2002; Sava and Biondi, 2004). A key element that is necessary for image-domain finite-frequency inversion methods is the analysis of subsurface image gathers. Extended images (EI's; see Sava and Vasconcelos, 2010), as we describe in this paper, are an extension of traditional subsurface-domain image gathers. As such, our objective with this paper is to provide formalism and insight regarding one- and two-way EI's that will serve as the basis for the development of image-domain inversion approaches.

Most wave-equation-based imaging methods rely on the cross-correlation of source and receiver wavefields to invoke the zero time-lag and zero space-lag imaging condition (e.g., Claerbout, 1971,1985). This imaging condition has recently been extended by correlating wavefields with non-zero lags in the spatial coordinates also (Sava and Fomel, 2003). This allows, for example, studying the dependence of the image gathers on the velocity used in wave-equation-based imaging. Besides allowing for lags in the spatial coordinates when calculating the cross correlations, one can also allow for non-zero lags in the time variable (Rickett and Sava, 2002; Sava and Fomel, 2006; Sava and Vasconcelos, 2009). We refer to the images obtained using non-zero lags in both the spatial and time variables as extended images.

In seismic interferometry the cross-correlation of wavefields received at two receivers allows the extraction of the response between these receivers as if one of them acts as a source (e.g., Claerbout, 1968; Fink, 1997; Rickett and Claerbout, 1999; Weaver and Lobkis, 2001; Campillo and Paul, 2003; Wapenaar, 2004; Schuster et al., 2004; Curtis et al., 2006; Wapenaar et al., 2006, and references therein; Wapenaar et al., 2010). Representation theorems for the scattered field traveling from one point inside the medium to another can be found using scattering reciprocity relations (Wapenaar, 2007; Wapenaar et al., 2008; Vasconcelos et al., 2009). These theorems contain surface integrals like those used in seismic interferometry. Since an image of a scatterer can be obtained by collapsing the recorded scattered wavefield onto the scatterer location, this formulation based on scattering representations can be used to interpret the imaging condition in the context of seismic interferometry (Vasconcelos, 2008): the image is the zero-time scattered-wave response generated by zero-offset pseudo-experiments in the image domain. Here we expand on this notion of "image-domain interferometry" and show that the representation theorems for the scattered field allow the extended images to be described as scattered wavefields which are "excited" and recorded in the image domain. We show this for both the one-way and two-way wave equation formulations.

While explicitly defining EI's from exact two- and one-way scattering reciprocity theorems is the essence of our work in this manuscript, the integral representations as used for seismic interferometry are not entirely new to seismic imaging. Esmersoy and Oristaglio (1988) and Oristaglio (1989) used reciprocity integrals to formulate the wavefield extrapolation step in reverse-time double-focussing migration algorithms, while de Hoop and de Hoop (1995) also used general reciprocity relations to describe the data redatuming for imaging of general acoustic, elastic and electromagnetic fields. In the context of linear, Born-based migration/inversion reciprocity relations have also been used to describe wavefield extrapolation both for two-way (e.g., Clayton and Stolt, 1981; Stolt and Weglein, 1985) and one-way (e.g., Wapenaar et al., 1989; Thorbecke and Berkhout, 2006) imaging. Furthermore, van Manen et al. (2006) were the first to point out the relationship between seismic interferometry and the migration resolution function, which was then developed in detail by Thorbecke and Wapenaar (2007). Vasconcelos (2008) then followed with an explicit general representation of Claerbout's imaging condition (e.g., Claerbout, 1971, 1985) using scattering-based integral relations originally derived for seismic interferometry (Vasconcelos and Snieder, 2008; Vasconcelos et al., 2009a). More recently, Halliday and Curtis (2010) derived the formal link between imaging by double-focussing (Oristaglio, 1989) in terms of the scattering-based version of the source-receiver interferometry method by Curtis and Halliday (2010).

In this manuscript, we further explore the connection first established by Vasconcelos et al. (2009b) between wave-equation imaging and seismic interferometry for general scattering experiments for two-way as well as one-way propagation. We begin our discussion by defining EI's for both two- and one-way imaging explicitly as time- and space-dependent subsurface scattering experiments. Next, we use reciprocity theorems for two- (Vasconcelos et al., 2009a) and one-way scattering (Wapenaar et al., 2008) to provide formal description for the extended imaging conditions. We describe how to generate two- and one-way EI's both in terms of wavefield extrapolation step as well as in terms of evaluating the imaging conditions. Finally, we address the computation of EI's in the context of the single-scattering assumption and connect our reciprocity-based formulation to current practice in two- and one-way migrations.

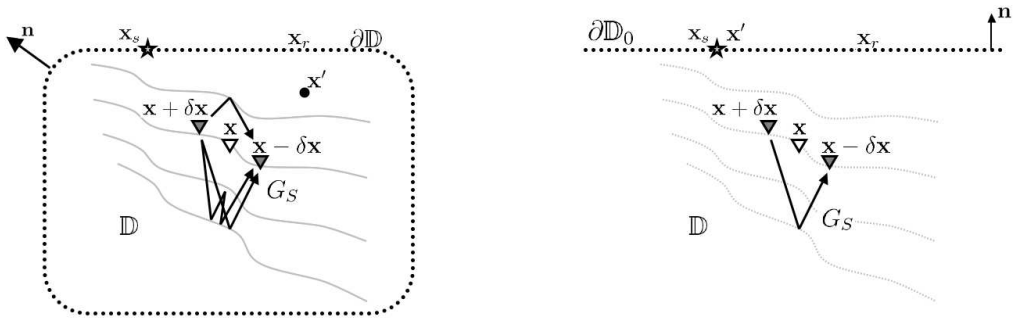

(a) **(b)**

Figure 1. Cartoons illustrating geometries for two-way extended imaging using scattering reciprocity. The point $\mathbf{x}$ (white triangle) is an image point in the subsurface/model domain $\mathbb{D}$. The points $\mathbf{x}+\delta\mathbf{x}$ and $\mathbf{x}-\delta\mathbf{x}$ (grey triangles) are respectively the locations of pseudo-sources and pseudo-receivers in $\mathbb{D}$, that are displaced from $\mathbf{x}$ by a space lag $\delta\mathbf{x}$. $\mathbf{x}_s$ and $\mathbf{x}_r$ represent, respectively, the locations of the physical sources (stars) and receivers (black dots) used in the data acquisition. For each shot in $\mathbf{x}_s$, there are receivers $\mathbf{x}_r$ everywhere on $\partial\mathbb{D}$ or $\partial\mathbb{D}_0$; and the sources themselves also cover the same surfaces. The arrows represent the scattered-wave response G_S. The curved grey lines represent heterogeneity in the subsurface model (e.g., layering). Panel (a) depicts the most general case where the surface $\partial\mathbb{D}$ encloses the subsurface domain and the imaging-condition integration is conducted over $\mathbf{x}'$ in the volume $\mathbb{D}$ as well as on the surface. In panel (a), the subsurface model may contain sharp boundaries which are indicated by the solid grey lines. Panel (b) depicts the more conventional configuration for single-scattering, Born-based imaging where integration is typically conducted over $\mathbf{x}'$ on the open surface $\partial\mathbb{D}_0$, and where sharp model discontinuities are absent (indicated by the dashed grey lines).

2 DEFINING A WAVEFIELD-BASED IMAGE

2.1 Two-way extended images

An imaging condition for migration by wavefield extrapolation can be defined in terms of a scattered field G_S, as (Claerbout, 1971)

$$\mathcal{I}(\mathbf{x}) = G_S(\mathbf{x},\mathbf{x},\tau=0)\,. \tag{1}$$

According to this definition, the conventional image $\mathcal{I}(\mathbf{x})$ can be physically thought of a zero-offset scattered field for source and receiver coinciding at the image point $\mathbf{x}$, evaluated at zero time. Since waves in the subsurface travel with finite wavespeeds, the zero-offset scattered-wave response in equation 1 is zero when $\mathbf{x}$ is away from scatterers or interfaces, and it is finite when the image point is at a scatterer or interface. Thus, it is the principle of causality that makes the image in equation 1 physically suitable for the mapping of discontinuities in the subsurface.

Based on the definition in equation 1, an extended image (EI) can be readily defined by evaluating the scattered field G_S for finite source-receiver offsets and at nonzero times, that is

$$\mathcal{I}_e(\mathbf{x},\delta\mathbf{x},\tau) = G_S(\mathbf{x}+\delta\mathbf{x},\mathbf{x},\tau)\,, \tag{2}$$

where $\delta\mathbf{x}$ and τ can be thought of as space and time lags, respectively. Note that equation 2 states that the extended image $\mathcal{I}_e$ corresponds to the scattered-wave response excited by a source at the image point $\mathbf{x}$ and recorded by receivers at $\mathbf{x}+\delta\mathbf{x}$ at time τ. Since there are no real physical excitations or observations inside the subsurface, we shall from now on refer to them as "pseudo-sources" and "pseudo-receivers". In addition, it is possible to define other types of extended images with "pseudo-acquisition" geometries that are different than that in equation 2. While $\mathcal{I}_e$ in equation 2 represents a common-source-type geometry, defining $\mathcal{I}_e(\mathbf{x},\delta\mathbf{x},\tau) = G_S(\mathbf{x}+\delta\mathbf{x},\mathbf{x}-\delta\mathbf{x},\tau)$ generates a common-mid-point type of geometry, where the conventional image point $\mathbf{x}$ lies at the midpoint between pseudo-sources at $\mathbf{x}-\delta\mathbf{x}$ and pseudo-receivers at $\mathbf{x}+\delta\mathbf{x}$. An illustration of the latter can be found in figure 1. Equations 1 and 2 identify an image as a scattered wavefield, i.e., as a space- and time-dependent object that satisfies the partial differential equation (PDE)

$$\hat{\mathcal{L}}\,\hat{\mathcal{I}}_e = -\mathcal{V}\,\hat{G}_0\,, \tag{3}$$

where $\hat{G}_0$ are frequency-domain Green's functions, $\hat{\mathcal{L}}(\mathbf{x})$ is a wave-equation operator, e.g., $\hat{\mathcal{L}}(\mathbf{x}) = \nabla^2 + c^{-2}(\mathbf{x})\;\omega^2$, and $\mathcal{V}(\mathbf{x})$ is a scattering operator, e.g., given $\hat{\mathcal{L}}_0(\mathbf{x}) = \nabla^2 + c_0^{-2}(\mathbf{x})\;\omega^2$, $\mathcal{V} = \hat{\mathcal{L}}(\mathbf{x}) - \hat{\mathcal{L}}_0(\mathbf{x}) = \omega^2\left[c^{-2}(\mathbf{x}) - c_0^{-2}(\mathbf{x})\right]$. Here, $c(\mathbf{x})$ and $c_0(\mathbf{x})$ pertain to the perturbed and reference subsurface wavespeed models, respectively. Since it follows from the definition of $\mathcal{V}$ that $\mathcal{L} = \mathcal{L}_0 + \mathcal{V}$, we point out that $\hat{\mathcal{I}}_e$ in equation 3 is nonlinear on $\mathcal{V}$. This means that the extended images

based on the definitions in equations 1 through 3 properly take the effects of multiple scattering into account.

It is important to note that the scattering potential $\mathcal{V}$ can be defined arbitrarily. The most common definition in migration/imaging literature (e.g., Oristaglio, 1989; Weglein, 2003; Symes, 2009) is that $c = c_0 + \delta c$ is comprised of a smooth background c_0 and of sharp discontinuities δc (i.e., the singular part of the model). Under this definition, $\mathcal{V}$ thus becomes an operator that accounts for the singularities in the scattered wavefields G_S. We will also use this definition in the context of this manuscript, but we point out that $\mathcal{V}$ can also be defined in other ways, e.g., as a smooth time-lapse change, or by incorporating attenuation (e.g., Vasconcelos et al., 2009).

2.2 One-way extended images

In the context of one-way wave propagation (e.g., Claerbout, 1971; Fishman and McCoy, 1984; Wapenaar et al., 2001; de Hoop et al., 2003), an extended image can be defined as

$$I_e(\mathbf{x}, \delta\mathbf{x}, \tau) = R_0^+(\mathbf{x} + \delta\mathbf{x}, \mathbf{x}, \tau)\,. \tag{4}$$

where $R_0^+(\mathbf{x}+\delta\mathbf{x}, \mathbf{x}, \tau)$ is the finite-time up-going reflectivity response to a downgoing field p^+ (Wapenaar et al., 2004; Wapenaar et al. 2008), for pseudo-sources at the image point $\mathbf{x}$ and pseudo-receivers at $\mathbf{x} + \delta\mathbf{x}$ within the subsurface (see figure 2). Similar to the definition of two-way extended images in terms of G_S in equation 2, the image I_e is also a space- and time-dependent, wavefield-like object. As with the two-way case, equation 4 is a straightforward extension of the classical definition of a subsurface image as a zero-offset and zero-time reflectivity response (e.g., Claerbout, 1971), i.e. $I(\mathbf{x}) = R_0^+(\mathbf{x}, \mathbf{x}, \tau = 0)$.

Despite the similarities in their definitions, the one-way extended image defined via equation 4 is fundamentally different from the two-way image defined in equation 2. The first and most important difference lies in the meaning of these definitions. While it follows from the definition of the two-way EI in equation 2 that $\mathcal{I}_e$ satisfies the PDE in equation 3, the one-way I_e in equation 4 is the kernel operator of the integral equation (e.g., Wapenaar et al., 2004; Wapenaar et al. 2008)

$$\hat{p}^-(\mathbf{x}_d, \mathbf{x}_s, \omega) = \int_{\mathbf{x}_z \in \partial\mathbb{D}_d} \hat{R}_0^+(\mathbf{x}_d, \mathbf{x}_z, \omega)\hat{p}^+(\mathbf{x}_z, \mathbf{x}_s, \omega) d^2\mathbf{x}_z; \tag{5}$$

where $\{\mathbf{x}_d, \mathbf{x}_z\}$ are points in the subsurface plane $\partial\mathbb{D}_d$, and $\hat{p}^-(\mathbf{x}_d, \mathbf{x}_s, \omega)$ and $\hat{p}^+(\mathbf{x}_z, \mathbf{x}_s, \omega)$ are respectively up- and down-going fields recorded at depth due to sources at $\mathbf{x}_s$ on the surface plane $\partial\mathbb{D}_0$. This is illustrated in figure 2. The EI in equation 4 is obtained from $\hat{R}_0^+(\mathbf{x}_d, \mathbf{x}_z, \omega)$ by choosing $\mathbf{x}_z = \mathbf{x}$ and $\mathbf{x}_d = \mathbf{x} + \delta\mathbf{x}$ and after an inverse Fourier transform $\omega \mapsto \tau$. Therefore, while the two-way EI $\mathcal{I}_e$ in equation 2 is a scattered wavefield with physical dimensions (e.g., dimensions of pressure), its one-way counterpart I_e in equation 4 is a dimensionless operator. Furthermore, the decomposition that yields the up/down-separated fields $p^{+,-}$ imposes limitations on spatial aperture (e.g., leading to a decrease in accuracy toward horizontal directions) and ignores the effects of laterally-propagating or evanescent wave modes (e.g., Fishman and McCoy, 1984; Wapenaar et al., 2001); these restrictions do not apply to the two-way extended images described by equation 3. Finally, we note that the one-way EI describes only up-going, back-scattered responses between subsurface points, whereas the two-way EI defined in terms of G_S ideally retrieves both forward- and back-scattered waves with no directional restrictions. Therefore, while one-way EI's retrieve only upward propagating reflection responses, two-way EI's ideally can reconstruct both transmission and reflection responses between subsurface points.

3 EXTENDED IMAGES FROM SCATTERING RECIPROCITY

3.1 Two-way imaging conditions

After defining the two-way EI's according to equations 1 and 2, the next step is to formally define imaging conditions that retrieve images that comply to those definitions. Since our definitions rely on the retrieval of the scattered fields G_S, we can use integral scattering representations to obtain the desired images (e.g., Thorbecke and Wapenaar, 2007; Wapenaar, 2007; Vasconcelos, 2008; Vasconcelos et al., 2009b; Halliday and Curtis, 2010). These scattering representations are similar to those employed in seismic interferometry applications (e.g., Bakulin and Calvert, 2006; Wapenaar, 2007; Vasconcelos and Snieder, 2008).

The extended images $\mathcal{I}_e$ that follow from equation 2 can be obtained reconstructing the scattered field G_S for finite times and by allowing the source and receiver locations to be arbitrarily different (see discussion about equation 2 above). Assuming a common image point $\mathbf{x}$, we write the pseudo-source and receiver locations as $\mathbf{x} + \delta\mathbf{x}$ and $\mathbf{x} - \delta\mathbf{x}$ respectively (figure 1). Using the correlation-type scattering representation for G_S from Vasconcelos et al. (2009a) in equation 2 then gives (Vasconcelos et al., 2009b)

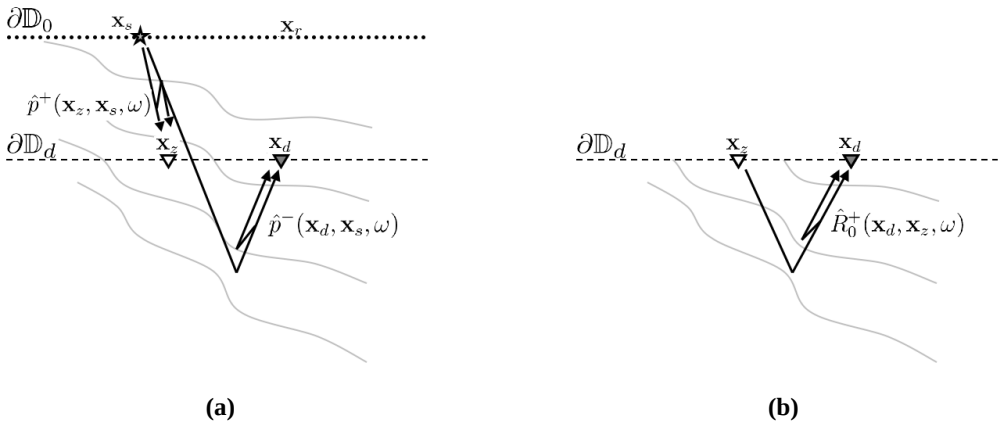

Figure 2. Cartoons illustrating geometries for one-way extended imaging using scattering reciprocity. As in Figure 1, $\mathbf{x}_s$ and $\mathbf{x}_r$ represent sources and receivers that cover the top acquisition surface $\partial\mathbb{D}_0$. $\mathbf{x}_z$ and $\mathbf{x}_d$ (depicted by triangles) are two arbitrary subsurface points that lie on the depth-domain surface $\partial\mathbb{D}_d$. In panel (a), $\hat{p}^{\pm}$ represent up- and down-going fields due to a source at $\mathbf{x}_s$ on $\partial\mathbb{D}_0$, and depth-extrapolated to $\partial\mathbb{D}_d$ from the data recorded by the receivers at all $\mathbf{x}_r \in \partial\mathbb{D}_0$ (black dots). $\hat{p}^{\pm}$ are the full up- or down-going wavefields that include all multiple arrival types. Panel (b) illustrates the up-going reflection impulse response $\hat{R}_0^+$ (equations 4 and 5) for a pseudo-source and a pseudo-receiver both on the depth-domain surface $\partial\mathbb{D}_d$, that contains all up-going primaries and multiples. Note that the response $\hat{R}_0^+$ corresponds to that of a medium that is heterogeneous below $\partial\mathbb{D}_d$ but is homogeneous above it.

$$
\begin{aligned}
\mathcal{I}_e(\mathbf{x},\delta\mathbf{x},\tau) \quad &= \quad G_S(\mathbf{x}-\delta\mathbf{x},\mathbf{x}+\delta\mathbf{x},t=\tau) \\
&= \int\Bigg(\oint_{\partial\mathbb{D}} \frac{F(\omega)}{i\omega\rho}\,\left[\nabla p_S(\mathbf{x}-\delta\mathbf{x},\mathbf{x}',\omega)\,p_0^*(\mathbf{x}+\delta\mathbf{x},\mathbf{x}',\omega)\right] \\
&\qquad\qquad \cdot\mathbf{n}\,d^2\mathbf{x}'\Bigg)\,e^{i\omega\tau}\,d\omega \\
&- \int\Bigg(\oint_{\partial\mathbb{D}} \frac{F(\omega)}{i\omega\rho}\,\left[p_S(\mathbf{x}-\delta\mathbf{x},\mathbf{x}',\omega)\,\nabla p_0^*(\mathbf{x}+\delta\mathbf{x},\mathbf{x}',\omega)\right] \\
&\qquad\qquad \cdot\mathbf{n}\,d^2\mathbf{x}'\Bigg)\,e^{i\omega\tau}\,d\omega \\
&+ \int\Bigg(\int_{\mathbb{D}} \frac{F(\omega)}{i\omega\rho}\,p(\mathbf{x}-\delta\mathbf{x},\mathbf{x}',\omega)\,\mathcal{V}(\mathbf{x}')\,p_0^*(\mathbf{x}+\delta\mathbf{x},\mathbf{x}',\omega) \\
&\qquad\qquad d^3\mathbf{x}'\Bigg)e^{i\omega\tau}\,d\omega\,; \qquad (6)
\end{aligned}
$$

where ρ is density, p_0 is a reference pressure field, p_S are scattered pressure waves and $p = p_0 + p_S$. $F(\omega)$ is a deconvolution-type filter that turns the pressure fields p into impulse responses G. The pressure fields in the integrand require "sources" at $\mathbf{x}'$ to be everywhere on the surface $\partial\mathbb{D}$ as well as in the volume $\mathbb{D}$ (figure 1a). Also, the "observation" points $\mathbf{x}$ and $\mathbf{x}\pm\delta\mathbf{x}$ are also inside the model and do not correspond to physical recording locations. Since in practice we physically excite waves at $\mathbf{x}_s$ and record them at $\mathbf{x}_r$ on the boundary (figure 1), the wavefields in the integrands of equation 6 are obtained after wavefield extrapolation. We address the role of wavefield extrapolation in the next section. Halliday and Curtis (2010) also use equation 6 to arrive at a generalized formula for the scattered field for imaging where the p_S fields in the integrand are themselves replaced by another set of integrals in the context of the source-receiver interferometry formulation (Curtis and Halliday, 2010).

Once $\mathcal{I}_e$ is defined by equation 6, it is straightforward to obtain the conventional image $\mathcal{I}$ (equation 1) by setting constant $\delta\mathbf{x} = \mathbf{0}$ and $\tau = 0$, which thus yields

$$
\begin{aligned}
\mathcal{I}(\mathbf{x}) \quad &= \quad G_S(\mathbf{x},\mathbf{x},\tau=0) \\
&= \int\Bigg(\oint_{\partial\mathbb{D}} \frac{F(\omega)}{i\omega\rho}\,\left[\nabla p_S(\mathbf{x},\mathbf{x}',\omega)\,p_0^*(\mathbf{x},\mathbf{x}',\omega)\right]\cdot\mathbf{n}\,d^2\mathbf{x}'\Bigg)\,d\omega \\
&- \int\Bigg(\oint_{\partial\mathbb{D}} \frac{F(\omega)}{i\omega\rho}\,\left[p_S(\mathbf{x},\mathbf{x}',\omega)\,\nabla p_0^*(\mathbf{x},\mathbf{x}',\omega)\right]\cdot\mathbf{n}\,d^2\mathbf{x}'\Bigg)\,d\omega \\
&+ \int\Bigg(\int_{\mathbb{D}} \frac{F(\omega)}{i\omega\rho}\,p(\mathbf{x},\mathbf{x}',\omega)\,\mathcal{V}(\mathbf{x}')\,p_0^*(\mathbf{x},\mathbf{x}',\omega)\,d^3\mathbf{x}'\Bigg)\,d\omega\,. \qquad (7)
\end{aligned}
$$

Although here we refer to this equation as a "conventional" image, we note that typical implementations of two-way imaging by, e.g. reverse-time migration, do not use the formulation above. We elaborate further on the differences between current migration/imaging practices and the equations above later in this manuscript.

The gradients terms in the integrands of equation 6 imply an implicit requirement for acquiring data with sources and receivers of both monopole and dipole type (e.g., Fokkema and van den Berg, 1993; Wapenaar and Fokkema, 2006). Since dipole (i.e., particle velocity) sources and receivers are seldom available in real-life seismic surveys, it is convenient to use the far-field approximation $\nabla p\cdot\mathbf{n} \;=\; i\,\omega\,c^{-1}\,p$ (e.g., Wapenaar and

$$\hat{R}_0^+\left(\mathbf{x}_d, \mathbf{x}_z, \omega\right) =$$

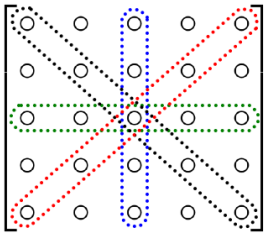

Figure 3. An illustration of the discrete operator $\hat{\mathbf{R}}_0^+ = \hat{R}_0^+(\mathbf{x}_d, \mathbf{x}_z, \omega)$ in matrix form, at a chosen $\partial\mathbb{D}_d$ (figure 2b) and for a fixed frequency ω. Each column of the matrix corresponds to a discrete pseudo-receiver location $\mathbf{x}_d$ and variable $\mathbf{x}_z$, whereas rows represent a fixed pseudo-source coordinate $\mathbf{x}_z$ and variable $\mathbf{x}_d$. The dotted contours highlight different choices of geometries of one-way extended images.

Fokkema, 2006) to recast equation 6 as

$$\begin{aligned}
\mathcal{I}_e(\mathbf{x}, \delta\mathbf{x}, \tau) \quad = \\
\int\Big(\oint_{\partial\mathbb{D}} \frac{2F(\omega)}{\rho c}\, p_S(\mathbf{x}-\delta\mathbf{x}, \mathbf{x}', \omega) \\
\qquad p_0^*(\mathbf{x}+\delta\mathbf{x}, \mathbf{x}', \omega)\Big) d^2\mathbf{x}'\, e^{i\omega\tau}\, d\omega \\
+\int\Big(\int_{\mathbb{D}} \frac{F(\omega)}{i\omega\rho}\, p(\mathbf{x}-\delta\mathbf{x}, \mathbf{x}', \omega)\, \mathcal{V}(\mathbf{x}') \\
\qquad p_0^*(\mathbf{x}+\delta\mathbf{x}, \mathbf{x}', \omega)\, d^3\mathbf{x}'\Big) e^{i\omega\tau}\, d\omega\,.
\end{aligned} \tag{8}$$

In the context of imaging conditions, as we point out above, the pressure fields in the integrands of equations 6 and 8 are obtained from wavefield extrapolation and not from direct physical experiments. When the fields in question are in fact direct measurements, then equations 6 and 8 above are the same as used for seismic interferometry applications (e.g., Bakulin and Calvert, 2006; Vasconcelos et al., 2009). It is important to note that in many of the interferometry applications (e.g., Bakulin and Calvert, 2006), the volume terms of equations 6 and 8 can be ignored (Vasconcelos et al., 2009a). For general imaging applications, however, the volume integrals cannot be ignored (Vasconcelos, 2008; Vasconcelos et al., 2009b; Halliday and Curtis, 2010). The connection between the calculation of extended images and seismic interferometry arises directly from the image definitions in equations 1 and 2 together with the use of scattering reciprocity integrals (e.g., Wapenaar, 2007; Vasconcelos, 2008; Vasconcelos et al., 2009b; Halliday and Curtis, 2010). A similar analogy exists for the one-way formulation as well (see below).

Given that the depth-domain fields $\hat{p}^-(\mathbf{x}_d, \mathbf{x}_s, \omega)$ and $\hat{p}^+(\mathbf{x}_z, \mathbf{x}_s, \omega)$ (equation 5 and figure 2) can be generated from the acquired data via wavefield extrapolation, extended images as defined in equation 4 can obtained by solving equation 5 for $\hat{R}_0^+$. The integral representation in equation 5 can also be expressed in discrete matrix-operator form, i.e., $\hat{\mathbf{P}}^- = \hat{\mathbf{R}}_0^+\,\hat{\mathbf{P}}^+$. Here the columns of the fixed-frequency matrices $\hat{\mathbf{P}}^\pm = \hat{\mathrm{P}}^\pm_{ij}$ contain $\hat{p}^\pm(\mathbf{x}, \mathbf{x}_i, \omega)$ for fixed source location $\mathbf{x}_i$ and variable receiver location $\mathbf{x}$, whereas the rows contain $\hat{p}^-(\mathbf{x}_j, \mathbf{x}, \omega)$ for fixed receiver location $\mathbf{x}_j$ and variable source location $\mathbf{x}$ at a particular fixed depth level. Figure 3 illustrates the operator $\hat{\mathbf{R}}_0^+ = \hat{R}_0^+(\mathbf{x}_d, \mathbf{x}_z, \omega)$ as a matrix for a chosen frequency.

A pseudo-inverse reflectivity operator $\bar{\mathbf{R}}_0^+$ can then be obtained from e.g. a regularized least-squares inversion as (e.g., Hansen, 1997; Wapenaar et al., 2008)

$$\bar{R}_0^+(\mathbf{x}_d, \mathbf{x}_z, \omega) = \bar{\mathbf{R}}_0^+ = \mathbf{P}^-(\mathbf{P}^+)^\dagger \left[\mathbf{P}^+(\mathbf{P}^+)^\dagger + \epsilon^2\mathbf{\Lambda}\right]^{-1} \tag{9}$$

where † stands for the conjugate-transpose, $\mathbf{\Lambda}$ is a shaping/regularization operator and ϵ is a weighting factor. With appropriate choices for ϵ and $\mathbf{\Lambda}$, equation 9 can yield an acceptable estimate of the reflectivity operator, i.e., $\bar{\mathbf{R}}_0^+ \approx \hat{\mathbf{R}}_0^+$. To then obtain an extended image I_e (e.g., equation 4) from the reflectivity operator, one can simply select an appropriate subset of $\hat{\mathbf{R}}_0^+$. For example, selecting a row of the $\hat{\mathbf{R}}_0^+$ (green highlight in Figure 3) operator (figure 3) and choosing a fixed $\mathbf{x}_z = \mathbf{x}$ for variable $\mathbf{x}_d = \mathbf{x} + \delta\mathbf{x}$ yields precisely the extended image as defined by equation 4. This choice leads to an extended image of a common-source type of geometry, similarly to that discussed for the two-way case of equation 2. Conversely, extracting the columns of $\hat{\mathbf{R}}_0^+$ (blue highlight in Figure 3) would yield extended images with a pseudo-acquisition geometry of the common-receiver type. Another choice would be to extract the off-diagonal elements of $\hat{\mathbf{R}}_0^+$ (red highlight in Figure 3) by setting $\mathbf{x}_d = \mathbf{x} - \delta\mathbf{x}$ and $\mathbf{x}_z = \mathbf{x} + \delta\mathbf{x}$ for a fixed image point $\mathbf{x}$: this would then yield $I_e(\mathbf{x}, \delta\mathbf{x}, \tau) = R_0^+(\mathbf{x} - \delta\mathbf{x}, \mathbf{x} + \delta\mathbf{x}, \tau)$, i.e., an extended image with a common-midpoint type of geometry. This geometry would be the same as that of the two-way $\mathcal{I}_e$ described by equations 6 and 8 and illustrated in figure 1.

As with the two-way imaging conditions presented above, extended imaging based on the one-way reciprocity theorem in equation 5 is also directly related to the practice of seismic interferometry. Wapenaar et al. (2008) presented the method of interferometry by multidimensional deconvolution (MDD) that relies on equations 5 and 9 to estimate $\hat{\mathbf{R}}_0^+$ from observed up- and down-going fields.

The approach presented here is the same as that in Wapenaar et al. (2008) except that the fields used in the estimation of the reflectivity operator are depth extrapolated fields, as opposed to physically observed data as used in interferometry (figure 2).

4 WAVEFIELD EXTRAPOLATION FOR NONLINEAR EXTENDED IMAGES

4.1 Two-way extrapolation

While interferometry relies on observed fields p_0 and p_S (e.g., Bakulin and Calvert, 2006; Vasconcelos, 2008), in two-way wave-equation imaging (equation 8) these fields result from extrapolating (i.e., re-datuming) the fields recorded at the acquisition surface to the image point $\mathbf{x}$ (e.g., Claerbout, 1985; Sava and Vasconcelos, 2009). In imaging, $p_0(\mathbf{x},\mathbf{x}',\omega)$ (e.g. equation 8) are depth-extrapolated source wavefields, which translates to numerically solving the following initial value problem

$$\begin{cases} \hat{\mathcal{L}}_0\,\hat{p}_0 = 0, & \hat{p}_0 = \hat{p}_0(\mathbf{x},\mathbf{x}',\omega),\ \mathbf{x}\in\mathbb{D}\ \text{ and } \mathbf{x}'\in\mathbb{D}\cup\partial\mathbb{D}, \text{with} \\ p_0(\mathbf{x}_r,\mathbf{x}_s,t) = s(t)*\delta(\mathbf{x}_r-\mathbf{x}_s,\mathbf{x}_s,t) & \text{as I.C., for all } \mathbf{x}_{s,r}\in\partial\mathbb{D}; \end{cases} \tag{10}$$

where I.C. stands for "initial conditions", $\mathbf{x}_s$ and $\mathbf{x}_r$ are the acquisition source and receiver coordinates (figure 1a), δ is the Dirac delta, $s(t)$ is the time-domain source signature and $*$ stands for convolution. The problem in equation 10 is translated as forward modeling of each shot at $\mathbf{x}'=\mathbf{x}_s\in\partial\mathbb{D}$ to every point $\mathbf{x}$ inside $\mathbb{D}$ (figure 1a). In addition, based on the fields from surface sources recorded at every $\mathbf{x}\in\mathbb{D}$, the response from each $\mathbf{x}'$ *inside* $\mathbb{D}$ to every $\mathbf{x}\in\mathbb{D}$ must also be calculated. This latter step can be performed, for example, with the method by van Manen et al. (2005). Solving the initial value problem described by equation 10 results in the $\hat{p}_0(\mathbf{x},\mathbf{x}',\omega)$ fields required by the extended imaging condition in equation 8. This reference field p_0 is traditionally named "the source wavefield" in migration practice. The source wavefield calculation in equation 10 is analogous to that performed in current migration practice, with the additional step of modeling the response of sources that are also inside the subsurface. This additional step is necessary for the evaluation of the volume integral in equation 8.

The next step is to compute the scattered fields $\hat{p}_S(\mathbf{x},\mathbf{x}',\omega)$, or "the receiver wavefields", necessary for evaluating the integrands in equation 8. These are obtained by solving the boundary value problem

$$\begin{cases} \hat{\mathcal{L}}\,\hat{p}_S = -\mathcal{V}\,\hat{p}_0, & \hat{p}_S = \hat{p}_S(\mathbf{x},\mathbf{x}',\omega),\ \mathbf{x}\in\mathbb{D} \text{ and } \mathbf{x}'\in\mathbb{D}\cup\partial\mathbb{D}, \text{with} \\ \hat{p}_S(\mathbf{x}_r,\mathbf{x}_s,\omega) = \hat{d}^*_S(\mathbf{x}_r,\mathbf{x}_s,\omega) & \text{as B.C., for all } \mathbf{x}_{s,r}\in\partial\mathbb{D}. \end{cases} \tag{11}$$

where B.C. stands for "Boundary Conditions", which consist of $\hat{d}^*_S(\mathbf{x}_r,\mathbf{x}_s,\omega)$: the full, time-reversed scattered wavefield from the acquired common-shot data. It is important to note here that the receiver extrapolation approach in equation 11 differs from usual migration practice in three points. First, here the boundary value problem described in equation 11 solves the inhomogeneous PDE for scattered fields (e.g., equation 3) as opposed to a homogeneous wave equation (e.g. similar to that in equation 10). As a consequence, the source wavefield p_0 that resulted from solving the problem in equation 10 must in fact be used for extrapolating for the receiver or scattered wavefield p_S as described by the problem in equation 11. Second, receiver wavefield extrapolation according to equation 11 uses the operators $\mathcal{L}$ and $\mathcal{V}$ which differ from the smooth operator $\mathcal{L}_0$ used for the source wavefield (equation 10). In other words, the models used for source and receiver extrapolation are different. This allows for the modeling of multiples in the extrapolation of the receiver wavefields as the wavefields $\hat{p}_0$ and $\hat{p}_S$ are allowed to interact with the singularities in $\mathcal{L}$ and $\mathcal{V}$ (equation 11). Third, as with the source wavefield calculation above, the field $\hat{p}_S(\mathbf{x},\mathbf{x}',\omega)$ must be computed for $\mathbf{x}'\in\mathbb{D}$ in additional to surface sources only (i.e. $\mathbf{x}'=\mathbf{x}_s\in\partial\mathbb{D}$). In the formulation by Halliday and Curtis (2010), the extrapolation for the receiver wavefield p_S is analitically expressed in terms of scattering representation integrals (Vasconcelos et al., 2009a) and inserted into equation 6, as opposed to the boundary value problem approach we present here.

4.2 One-way extrapolation

Wavefield extrapolation for the generation of one-way extended images as discussed above is in fact similar to current practice in one-way migration. The depth-domain source wavefield $\mathbf{P}^+=\hat{p}^+(\mathbf{x}_z,\mathbf{x}_s,\omega)$ (equations 5 and 9) is generated via

$$\begin{cases} \mathbf{P}^+ = \mathbf{T}^+\,\mathbf{S}^+_0, & \text{with} \\ \mathbf{S}^+_0 = \hat{s}^+_0(\mathbf{x}_r,\mathbf{x}_s,\omega) = \delta(\mathbf{x}_r-\mathbf{x}_s,\mathbf{x}_s)\,s(\omega), & \text{for all } \{\mathbf{x}_s,\mathbf{x}_r\}\in\partial\mathbb{D}_0, \end{cases} \tag{12}$$

where $\mathbf{S}_0^+ = \hat{s}_0^+(\mathbf{x}_r, \mathbf{x}_s, \omega)$ are the source data at the acquisition surface (figure 2), $s(\omega)$ is the frequency-domain source excitation function and $\mathbf{T}^+$ is a modeling operator for down-going transmission that maps surface data at $\mathbf{x}_r \in \partial\mathbb{D}_0$ to subsurface-domain wavefields at $\mathbf{x}_z \in \partial\mathbb{D}_d$ (figure 2). In parallel with the source wavefield calculation in equation 12, the one-way receiver fields $\mathbf{P}^- = \hat{p}^-(\mathbf{x}_d, \mathbf{x}_s, \omega)$ (equations 5 and 9; figure 2) are obtained from

$$\begin{cases} \mathbf{P}^- = \left(\mathbf{T}^-\right)^{-1} \mathbf{D}_0^-, & \text{with} \\ \mathbf{D}_0^- = \hat{d}_0^-(\mathbf{x}_r, \mathbf{x}_s, \omega), & \text{for all } \{\mathbf{x}_s, \mathbf{x}_r\} \in \partial\mathbb{D}_0, \end{cases} \tag{13}$$

where $\mathbf{D}_0^- = \hat{d}_0^-(\mathbf{x}_r, \mathbf{x}_s, \omega)$ are the full, up-going reflection data acquired for all shots and receivers on the acquisition surface. $\mathbf{T}^-$ is the modeling operator for up-going transmission that datums depth-domain fields at all $\mathbf{x}_d \in \partial\mathbb{D}_d$ to surface data at $\mathbf{x}_r \in \partial\mathbb{D}_0$ (figure 2). The inverse of $\mathbf{T}^-$ thus maps the reflection data at the surface to the receiver wavefield in the subsurface.

There are three main distinctions between the wavefield extrapolation steps described by equations 12 and 13 and those employed in current one-way migration approaches. First, the up-going surface data $\mathbf{D}_0^- = \hat{d}_0^-(\mathbf{x}_r, \mathbf{x}_s, \omega)$ contains the full recorded reflection response (i.e., with all up-going multiples), as opposed to only primary reflection data. Second, the modeling operators $\mathbf{T}^{\pm}$ are meant to be full transmission response operators (e.g., Thorbecke, 1997; Wapenaar et al., 2004), i.e., they model amplitude-preserving transmitted fields that contain direct arrivals as well as transmission multiples. Malcolm et al. (2009) offers a scattering-series-based approach that can be used for practical implementation of the nonlinear $\mathbf{T}^{\pm}$ operators. Finally, we note that the inverse operator $\left(\mathbf{T}^-\right)^{-1}$ is used for the back-propagation of the receiver data $\mathbf{D}_0^-$, whereas common practice does not rely on inverse transmission operators (see next section). In principle, these three differences combined allow for the proper modeling of multiples in the depth-extrapolated fields, which is a key element necessary for the inversion of the full nonlinear reflectivity operator in equations 5 and 9. In the next section we address differences between the steps above and the computation of extended images in current migration practice.

5 EXTENDED IMAGES IN CURRENT MIGRATION PRACTICE

Unlike the discussion above on the nonlinear imaging conditions and on wavefield extrapolation that models multiples in the depth-extrapolated fields, most current migration practices generally rely on the Born approximation (e.g., Claerbout, 1971; Stolt and Weglein, 1985) for both one- and two-way imaging. Furthermore, since the objective behind most migration schemes is structural characterization, it is not uncommon that additional approximations are made that ignore amplitude-related effects in extrapolation and imaging. As a consequence, these approximations bring two major simplifications for practically implementing EI's, namely, *i*) that all of the wavefield extrapolation can be carried out with a single smooth wave-speed model and *ii*) that the evaluation of the imaging conditions is substantially simpler and becomes effectively the same for both two- and one-way imaging.

Two-way imaging in current migration practice is typically achieved first by adapting the receiver wavefield extrapolation in equation 11 to

$$\begin{cases} \hat{\mathcal{L}}_0\, \hat{p}_S = 0 & \text{for } \hat{p}_S(\mathbf{x}, \mathbf{x}', \omega) \text{ with } \mathbf{x} \in \mathbb{D}, \mathbf{x}' = \mathbf{x}_s \in \partial\mathbb{D}_0 \\ \hat{p}_S(\mathbf{x}_r, \mathbf{x}_s, \omega) = \hat{d}_P^*(\mathbf{x}_r, \mathbf{x}_s, \omega) & \text{for all } \mathbf{x}_{s,r} \in \partial\mathbb{D}_0; \end{cases} \tag{14}$$

where the primary-only data $\hat{d}_P(\mathbf{x}_r, \mathbf{x}_s, \omega)$ replaces the full recorded scattered waves $\hat{d}_S(\mathbf{x}_r, \mathbf{x}_s, \omega)$ in equation 11, and these are now backward-extrapolated with the smooth Helmholtz operator $\mathcal{L}_0$, same as used for the source wavefield extrapolation described by equation 10. We point out the homogeneous PDE $\hat{\mathcal{L}}_0\, \hat{p}_S = 0$ is not equivalent to the Born approximation of the inhomogeneous PDE in equation 11. Proper Born modeling would require the inclusion of the forcing term $-\mathcal{V}\hat{p}_0$, i.e., solving for $\hat{\mathcal{L}}_0\, \hat{p}_S = -\mathcal{V}\, \hat{p}_0$ instead. Sources and receivers are no longer assumed to enclose the medium, and are instead available only over a finite surface $\partial\mathbb{D}_0$ (figure 1b). While this assumption mimics realistic geophysical data where physical sources and receivers are only available at the Earth's surface, it also typically introduces artifacts in the wavefield reconstruction and interferometry processes (e.g., Wapenaar, 2006, Wapenaar and Fokkema, 2006). Note that here the responses of both source and receiver wavefields, i.e, $\hat{p}_{0,S}(\mathbf{x}, \mathbf{x}', \omega)$, are computed only for points $\mathbf{x}' = \mathbf{x}_s$ on the surface, while the fields extrapolated in equations 10 and 11 need additional extrapolated sources at the points $\mathbf{x}'$ inside the subsurface volume.

By extrapolating the receiver wavefield according to equation 14 as opposed to equation 11, the nonlinear interactions between the back-propagating receiver wavefield and the model discontinuities present in the operators $\mathcal{L}$ and $\mathcal{V}$ are ignored. Also, when ignoring the contributions of model discontinuities in the extrapolation step (i.e. by ignoring the Born forcing term $\mathcal{V}\, \hat{p}_0$), current two-way migration algorithms thus also ignore the volume integral in

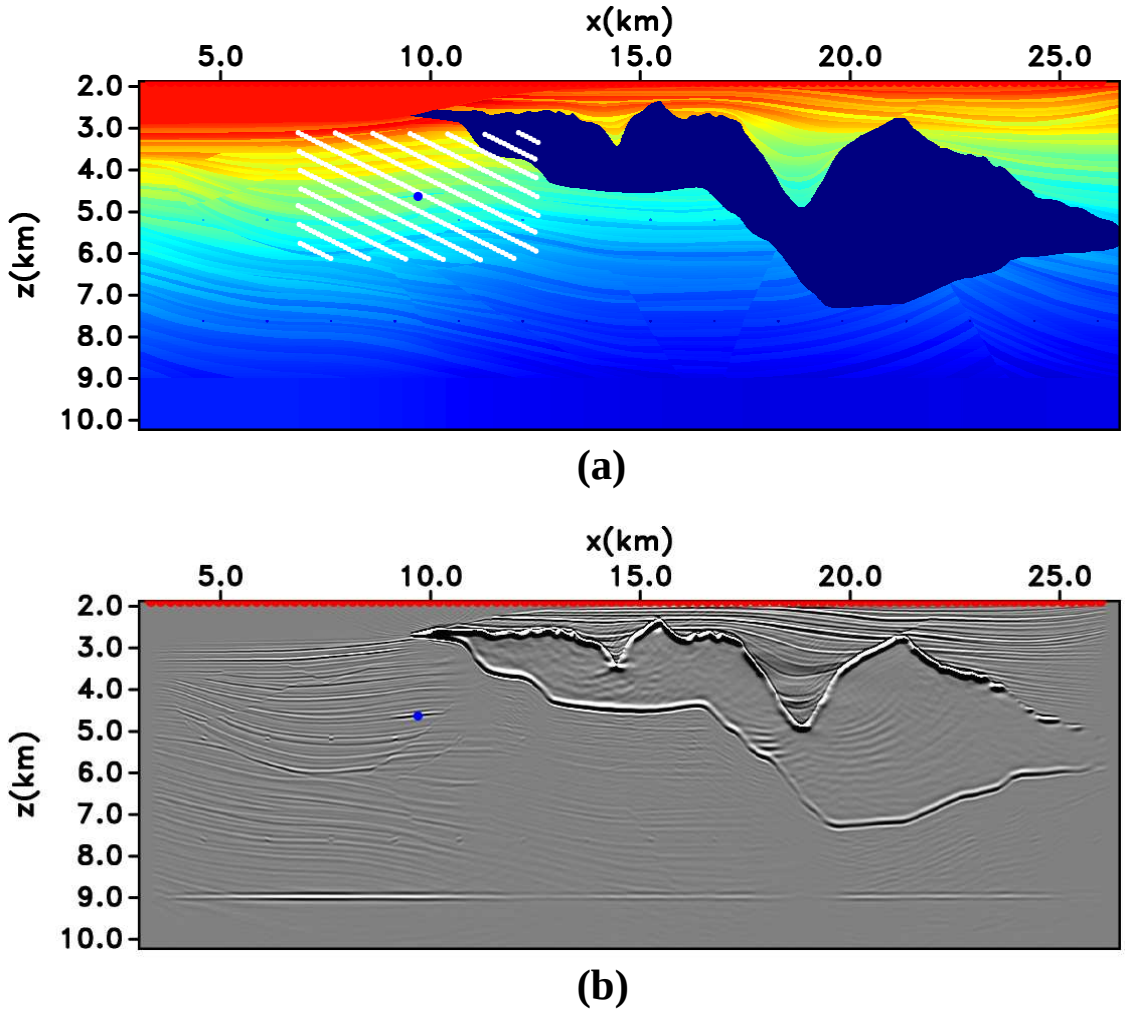

Figure 4. Sigsbee numerical example. Panel (a) shows the true wavespeed model, while panel (b) shows a conventional one-way migrated image. The blue dot in both panels shows the location $\mathbf{x}$ of the extended image portrayed in figure 5. The red dots show the location of the surface acquisition shots $\mathbf{x}_s \in \partial\mathbb{D}_0$. The area highlighted by white lines in panel (a) indicates the spatial coverage of space-lags $\delta\mathbf{x}$ in the extended image (figure 5). The EI in figure 5 is an approximate reconstruction of the scattered waves excited at $\mathbf{x}+\delta\mathbf{x}$ somewhere inside the white-highlighted area and recorded at $\mathbf{x}-\delta\mathbf{x}$. The original acquired data is laid out in a towed-streamer-type geometry whereby the recording receivers lie only on the right-hand side of the shots.

the imaging condition in equation 8. Thus, an EI can be approximated from equation 8 as the surface integral

$$\mathcal{I}_e(\mathbf{x},\delta\mathbf{x},\tau) \approx \int\left(\int_{\partial\mathbb{D}_\mathbf{0}} \frac{2F(\omega)}{\rho c}\, p_S(\mathbf{x}-\delta\mathbf{x},\mathbf{x}_s,\omega)\, p_0^*(\mathbf{x}+\delta\mathbf{x},\mathbf{x}_s,\omega) d^2\mathbf{x}_s\right) e^{i\omega\tau}\, d\omega\,;$$

where $\partial\mathbb{D}_\mathbf{0}$ is a subset of $\partial\mathbb{D}$ (figure 1), and $\mathbf{x}' = \mathbf{x}_s$ as shown in equation 14. This result yields an estimate for an EI that is a straightforward extension of the conventional correlation-based imaging condition, obtained by adding space lags $\delta\mathbf{x}$ and time lags τ to the cross-correlation of source wavefields p_0 and receiver wavefields p_S (Sava and Vasconcelos, 2009; Sava and Vasconcelos, 2010).

An analogous approach is taken to generate one-way EI's under the single-scattering approximation and using a smooth wavespeed model. For one-way imaging, source wavefield extrapolation is done according to equation 12 with the full transmission operator $\mathbf{T}^+$ replaced by $\mathbf{T}_0^+$, the transmission operator in a smooth medium (e.g., Thorbecke, 1997; Wapenaar et al., 2004). A similar replacement takes place in the receiver wavefield extrapolation, $\mathbf{T}^-$ is replaced by its smooth medium counterpart $\mathbf{T}_0^-$. Additionally, given the computational challenges involved with computing the inverse of the transmission operator (equation 13), $\left(\mathbf{T}_0^-\right)^{-1}$ is typically replaced by the conjugate-transpose $\left(\mathbf{T}_0^-\right)^\dagger$.

Once one-way source and receiver wavefields are extrapolated using the smooth transmission operators $\mathbf{T}_0^+$ and $\left(\mathbf{T}_0^-\right)^\dagger$, the image is estimated by cross-correlating the resulting source and receiver fields, i.e.,

$$\tilde{\mathbf{R}}_0^+ \approx \mathbf{P}^-(\mathbf{P}^+)^\dagger; \tag{15}$$

which is an approximation to the inverse in equation 9 (e.g., Claerbout, 1971; Wapenaar et al., 2008). The standard one-way migrated image is then extracted from the diagonal elements of $\tilde{\mathbf{R}}_0^+$ (black highlight in figure 3). From the $\tilde{\mathbf{R}}_0^+$ matrix (equation 15), EI's can be obtained by selecting other specific combinations of its elements, as discussed above discussion regarding figure 3. For example, the off-diagonal elements of $\tilde{\mathbf{R}}_0^+$ (highlighted in red in figure 3) yield the extended image $I_e(\mathbf{x},\delta\mathbf{x},\tau) = \tilde{R}_0^+(\mathbf{x}-\delta\mathbf{x},\mathbf{x}+\delta\mathbf{x},t=\tau)$, which based on equation 15 can be directly evaluated via the integral

$$\begin{aligned} I_e(\mathbf{x},\delta\mathbf{x},\tau) &= \tilde{R}_0^+(\mathbf{x}-\delta\mathbf{x},\mathbf{x}+\delta\mathbf{x},\tau) \\ &= \int\left(\int_{\partial\mathbb{D}_0} p^-(\mathbf{x}-\delta\mathbf{x},\mathbf{x}_s,\omega)\right. \\ &\quad \left.\{p^+(\mathbf{x}+\delta\mathbf{x},\mathbf{x}_s,\omega)\}^*\, d^2\mathbf{x}_s\right) e^{i\omega\tau} d\omega\,. \end{aligned} \tag{16}$$

Thus, in current one-way migration practice, we can readily generate an EI by adding space and time lags to the conventional cross-correlation of receiver and source wavefields (p^- and p^-, respectively, in equation 16), followed by a summation over sources $\mathbf{x}_s$ on the acquisition plane $\partial\mathbb{D}_0$.

Figures 4 and 5 provide a numerical example from the Sigsbee model of a one-way EI that is generated using equation 16. The standard image, displayed in figure 4b, corresponds to the diagonal elements of the estimated $\tilde{\mathbf{R}}_0^+$ matrix (equation 15), evaluated at $\tau = 0$. Because it is an approximate estimate of $\tilde{R}_0^+(\mathbf{x},\mathbf{x},\tau=0)$, the conventional image in figure 4b is commonly interpreted as a representation of the structure of the true model in figure 4a.

The EI in figure 5, however, shows that extended images display an appearance which is similar to that of recorded data, i.e., that of time- and space-dependent band-limited signals with characteristic moveout signatures. This is consistent with the reciprocity-based definitions of the EI as given by equations 4, 9, or 16, that show that an EI are reconstructed reflectivity data acquired by pseudo sources and receivers in the subsurface model. This "reconstruction" is analogous to data reconstruction by seismic interferometry (e.g., Wapenaar and Fokkema, 2006; Bakulin and Calvert, 2006), with the distinction that the computation of extended imaging conditions is done with extrapolated image-domain fields as opposed to actual recordings. While the reflectivity response reconstructed in the EI in figure 5 is predominantly causal as expected from the definition in equation 4, arrivals are also present for $\tau < 0$ due to the approximation made in using only the adjoint of $\mathbf{P}^+$ and not its inverse (see equations 9 and 15). Furthermore, the proper reflectivity moveout signatures are reconstructed only for $\tau > 0$ and $\lambda_x < 0$ because the towed-streamer acquisition of the Sigsbee synthetic data only allows for receivers to be placed on one side of the source locations.

6 DISCUSSION

In this paper, we define extended images (EI's) for both two- and one-way explicitly as scattered fields or, respectively, reflectivity operators that are both excited and recorded within the subsurface and for finite times. These definitions for "an image" (e.g., according to equations 2 and 4), while consistent with the concepts originally offered by Claerbout (e.g., 1971, 1985), differ from the majority of formal definitions for an image which target the direct reconstruction of discontinuities in the Earth parameters, e.g. the scattering potential $\mathcal{V}$ (e.g., Prosser, 1968; Beylkin, 1984; Stolt and Weglein, 1985; Esmersoy and Oristaglio, 1988; Weglein et al., 2003; Symes, 2008). Instead, by defining EI's in terms of space- and time-dynamic objects such as the two-way wavefield G_S, or the one-way reflectivity operator R_0^+ we use wavefield reciprocity (e.g., Fokkema and van den Berg, 1993; Wapenaar et al., 2008; Vasconcelos et al., 2009) to derive formal expression for the nonlinear extended imaging conditions as presented in this manuscript.

By invoking integral reciprocity relations and defining EI's as subsurface-domain scattering experiments, we draw an explicit connection between the computation of extended images via migration-type imaging by wavefield extrapolation and current practices in seismic interferometry. In fact, the integral representations we propose here for generating EI's are precisely the same as those employed in seismic interferometry. The scattering representation we use for our two-way extended imaging condition is directly analogous to that employed in scattered-wave seismic interferometry as discussed by, e.g., Bakulin and Calvert (2006); Vasconcelos et al. (2009a) and Wapenaar et al. (2010). Likewise, our one-way EI formulation is based on the one-way approach by Wapenaar et al. (2008).

When the imaging objective is structural characterization, it is common for current migration practice to rely on the single-scattering approximation and to ignore amplitude effects. In that case, we show here that the two- and one-way extended imaging conditions are essentially the same calculation (described by equations 15 and 16): a straightforward cross-correlation of receiver and source depth-domain wavefields followed by summing over all shots on the acquisition surface. The only difference being that the source and receiver wavefields are generated via two- or one-way extrapolation. This explicitly connects our formulation to common practice in migration-type imaging widely employed today. We point out, however, that this similarity be-

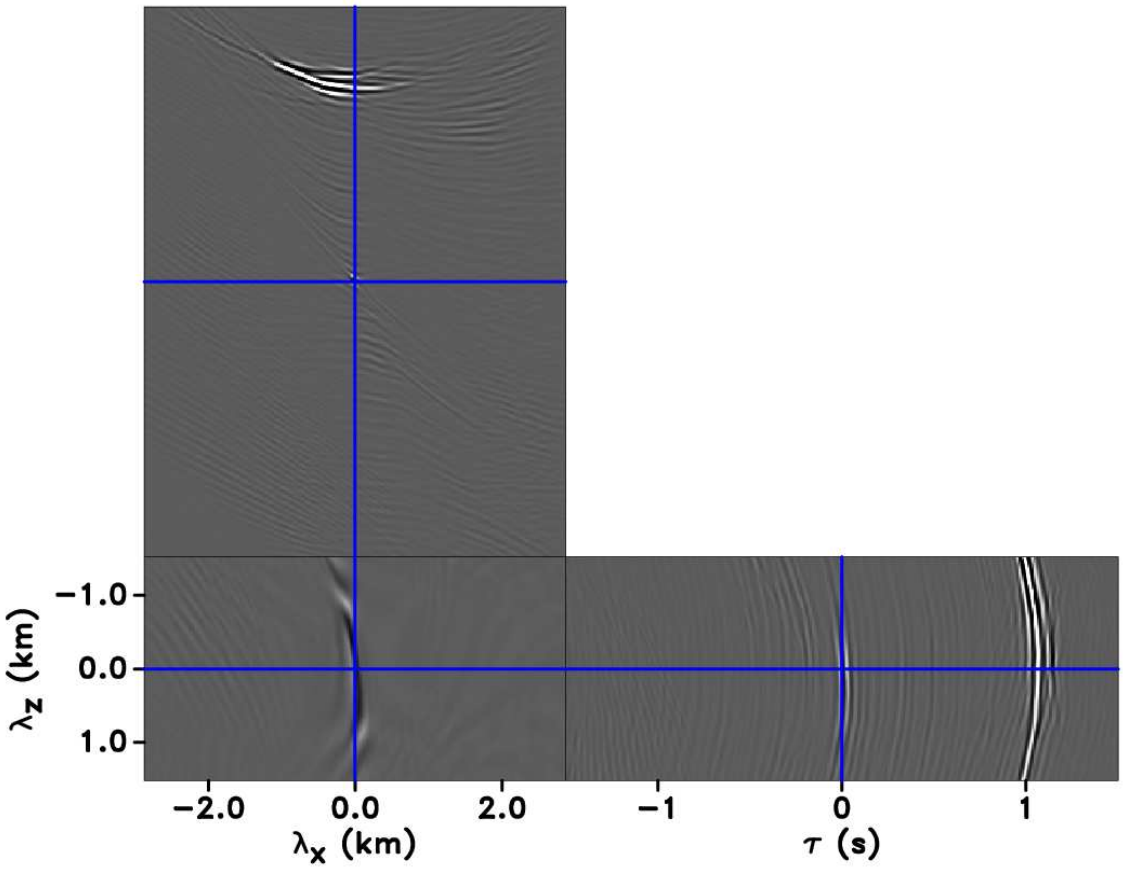

Figure 5. Example of a one-way, fully extended image (EI) of common-mid-point type of geometry, i.e., $I_e(\mathbf{x}, \delta\mathbf{x}, \tau) = \tilde{R}_0^+(\mathbf{x} - \delta\mathbf{x}, \mathbf{x} + \delta\mathbf{x}, t = \tau)$. The EI is shown here for a fixed $\mathbf{x}$-location (indicated by the blue dot in figure 4), and for varying $\delta\mathbf{x}$ and τ. The space-lag $\delta\mathbf{x}$ has components $\{\lambda_x, \lambda_z\}$ which are shown in the figure axes. τ-axis is the time-lag variable.

tween two- and one-way EI's exhibited by equations 15 and 16 is only due to the approximations involved. In their more general form, reciprocity-based two-way EI's are substantially different from their one-way counterparts both in terms of their meaning as well as in terms of the required computations. These differences, however, should only necessarily be addressed in imaging practice if the objective is to deal with nonlinear effects in the imaging process such as e.g. the migration of multiples or amplitude corrections due to transmission effects. Consistently with our findings, Halliday and Curtis (2010) show that Oristaglio's (1989) two-way inversion formula, which is a Born-inversion extension to Claerbout's imaging condition (1971), explicitly follows from interferometry-based integral relations.

Since the reciprocity-based integrals used for interferometry make no single-scattering assumptions and in principle reconstruct full nonlinear scattering responses, our imaging conditions based on image-domain interferometry are suitable for dealing with nonlinear imaging such as multiple-scattered arrivals and associated amplitude effects. To properly account for nonlinear effects in both the two- and one-way case, current extrapolation practices must be modified such that nonlinearity is accounted for at the modeling stage. We show here that while nonlinear transmission operators must be used for both source and receiver wavefields in one-way imaging, in the two-way approach only the receiver wavefields include nonlinear effects and their modeling becomes dependent on previously computed source wavefields.

Apart from the necessary modifications in the wavefield extrapolation step, we show that the imaging conditions that generate nonlinear EI's also differ from standard migration practice. In the two-way case, apart from the evaluation of a surface integral of cross-correlated source and receiver wavefields (akin to the source stacking typically conducted in shot-profile migration) there is an extra volume integral term that must be evaluated. Concurrent with our analysis, Halliday and Curtis (2010) show that the volume terms are necessary both for nonlinear imaging as well as for imaging based on Born inversion (Oristaglio, 1989). While there is no volume integral term to be computed in generating one-way EI's, these in turn require the in-

version of the full source-wavefield data matrix. At this point, computing the two-way volume integral or one-way data matrix inverse both present unsolved computational challenges in practically computing nonlinear EI's. These issues are currently the subject of further investigation.

It is important to emphasize that the greatest challenge in practically computing nonlinear EI's is, at the same time, the main justification for why we should generate them in the first place. As shown in the approach we provide in this manuscript, the computation of both two- and one-way EI's requires knowledge not only of the smooth migration velocity model, but also of the discontinuities (i.e., the singularities) in the subsurface model. That information is obviously not available at the outset of a seismic imaging experiment. It is precisely for the determination of velocity models, e.g., via wave-equation image-domain inversion approaches, that the concept of image extensions was originally developed. Symes (2008, and references therein) provides a comprehensive description of the role of extended images in the velocity inversion problem within the context of differential semblance optimization.

Sava and Vasconcelos (2010) show that EI's can bring additional sensitivity to the wavespeed models used in current migration practice, and can help in advancing migration-based methods for the inversion of background wavespeed models. While using EI's in current migration schemes is in itself potentially beneficial for increasing sensitivity to background migration wavespeed models, our nonlinear EI formulation presented here can be used to devise nonlinear finite-frequency inversions whose objective functions act in the subsurface image domain. Such approaches would bring the advantages of using image extensions and differential semblance as advocated by Symes (2008) to designing practical numerical solutions to the nonlinear seismic inverse scattering problem (e.g., Tarantola, 1984; Rose et al., 1985; Weglein et al., 2003; Symes, 2009). We note also that Halliday and Curtis (2010) show that the scattering-based EI's as presented here are formally connected to exact Born inverse scattering formulations and are thus also suitable for extensions to more sophisticated nonlinear problems.

On a more practical note, we point out that the EI formulation we present here can immediately contribute to current migration routines. For instance, recent examples of two-way reverse-time migration applications that utilize sharp boundaries in the migration velocity model to migrate multiply-scattered arrivals (e.g., Fletcher et al., 2006; Guitton et al., 2006; Jones et al., 2007) rely on a conventional migration practices and do not evaluate the volume integral term in the two-way imaging condition. Our approach for generating two-way reciprocity-based images can be implemented for the imaging of multiple-scattered arrivals using interpretation-based wavespeed models containing sharp discontinuities, i.e., by using sharp horizons picked from pre-existing images and using our two-way formulation to adapt a reverse-time migration scheme. Likewise, our one-way nonlinear EI formulation based on multi-dimensional deconvolution is readily applicable to one-way migrations that rely on amplitude-preserving one-way extrapolators (e.g., Zhang et al., 2007) or to recursive one-way migrations that target the imaging of multiples (e.g., Berkhout and Verschuur, 2006; Malcolm et al., 2009).

7 CONCLUSIONS

Extended images (EI's) in wavefield seismic imaging can be explicitly defined as space- and time-dependent objects in the subsurface domain. In our particular case, we define EI's as time-varying scattered wavefields that are excited and acquired by virtual sources and receivers that surround a particular image point in the subsurface domain. This definition of an EI departs from the typical concept of migrated image as a static representation of the discontinuities in the Earth's subsurface. Two-way EI's are defined as scattered fields that satisfy the partial differential equation for scattering in the subsurface domain, whereas we define one-way EI's as a dimensionless reflectivity operator that relates down-going excitations with the up-going subsurface waves recorded in the data.

Together with exact integral reciprocity relations, our definitions of two- and one-way EI's reveal an immediate connection between wave-equation imaging and the practice of seismic interferometry. Our extended images are, in fact, interferometric reconstructions of two- or one-way scattering experiments that use model-dependent, depth-extrapolated data as opposed to physically observed recordings typically employed in seismic interferometry. Because we use the same general scattering reciprocity integrals used in interferometry to define EI's, we expect that both our two- and one-way formulations for the extended imaging conditions account for nonlinear amplitude and multiple scattering effects.

To migrate multiples or to account for other nonlinear imaging effects, the computation of EI's departs significantly from today's practices in wave-equation migration. First, the depth-extrapolation step must be appropriately modified to model scattering interactions with model discontinuities: only for the receiver wavefields in two-way imaging, and for both source and receiver wavefields in the one-way case. Next, we show that the imaging condition for two-way reciprocity-based EI's requires the inclusion of an additional scattering volume integral term that is not present in typical migration routines. In the one-way case, the extended imaging condition requires the inversion of the full down-going source-wavefield data matrix, which departs from current approaches that use either cross-correlation or single-channel deconvolution.

Our explicit reciprocity-based descriptions of two- and one-way EI's can be used to address, both analytically as well as numerically, the velocity-dependent signatures of these fully extended image gathers. Consequently, these wavefield-based EI's can help in devising general formulations of image-domain objective functions for finite-frequency velocity inversion. In addition, one- and two-way EI's as we describe here can be of immediate use in current reverse-time migration applications, as well as in refining amplitude-preserving one-way wave-equation migration routines.

8 ACKNOWLEDGEMENTS

We thank ION/GXT for supporting this work and granting the permission to publish it. P. Sava thanks the sponsors of the CWP consortium for financial support. I. Vasconcelos is thankful to Andrew Curtis (Edinburgh University) and David Halliday (Schlumberger) for sharing their material on source-receiver interferometry and imaging.

REFERENCES

A. Bakulin and R. Calvert, 2006, The virtual source method: Theory and case study: Geophysics, **71**, SI139–SI150.

G. Beylkin, 1985, Imaging of discontinuities in the inverse scattering problem by inversion of a causal generalized radon transform. J. Math. Phys., **26**, 99–108.

A.J. Berkhout and D.J. Verschuur, 2006, Imaging of multiple reflections: Geophysics, **71**, SI209–SI220.

D.E. Budreck and J.H. Rose, 1990, Three-dimensional inverse scattering in anisotropic elastic media, *Inverse Problems*, **6**, 331–348.

M. Campillo and A. Paul, 1997, Long-range correlations in the diffuse seismic coda, *Science*, **299**, 547–549.

H. Chauris , 2000, *Analyse de vitesse par migration pour l' imagerie des structures complexes en sismique réflexion.* PhD Thesis, École des Mines de Paris.

J.F. Claerbout ,1968, Synthesis of a layered medium from its acoustic transmission response. *Geophysics*, **33**, 264–269.

J.F. Claerbout, 1971, Toward a unified theory of reflector mapping. Geophysics, **36**, 741–768.

J.F. Claerbout, 1985, Imaging the Earth's Interior. Blackwell Scientific Publishers, Oxford.

R.W. Clayton and R.H. Stolt, 1981, A Born-WKBJ inversion method for acoustic reflection data, *Geophysics*, **46**, 1559–1567.

A. Curtis, P. Gerstoft, H. Sato, R. Snieder and K. Wapenaar, 2006, Seismic interferometry – turning noise into signal: The Leading Edge, **25**, 1082–1092.

A. Curtis and D. Halliday, 2010, Source-receiver wavefield interferometry. *submitted*.

M.V. de Hoop and A.T. de Hoop, 1999, Wave-field reciprocity and optimization in remote sensing, *Proc. R. Soc. Lond.*, **456**, 641–682.

M. de Hoop, R. van der Hilst and P. Shen, 2006, Wave-equation reflection tomography: annihilators and sensitivity kernels, *Geophys. J. Intl.*, **167**, 1332–1352.

C. Esmersoy and M. Oristaglio, 1988, Reverse-time wavefield extrapolation, imaging and inversion, *Geophysics*, **53**, 920–931.

M. Fink, 1997, Time-reversed acoustics, *Physics Today*, **50**, 34–40.

L. Fishman and J.J. McCoy, 1984, Derivation and extension of parabolic wave theories. I. The factorized Helmholtz equation, *J. Math. Phys.*, **25**, 285–296.

L. Fishman, J.J. McCoy and S.C. Wales, 1987, Factorization and path integration of the Helmholtz equation: Numerical algorithms, *J. Acoust. Soc. Am.*, **81**, 1355–1376.

R.P. Fletcher, P.J. Fowler, P. Kitchenside and U. Albertin, 2006, Suppressing unwanted internal reflections in prestack reverse-time migration, *Geophysics*, **71**, E79–E82.

J.T. Fokkema and P.M. van den Berg. Seismic applications of acoustic reciprocity. *Elsevier Service Publishing Co.*, 1993.

D. Halliday and A. Curtis, 2010, An interferometric theory of source-receiver scattering and imaging. *submitted*.

P.C. Hansen, 1997, Rank-deficient and discrete ill-posed problems: numerical aspects of linear inversion, *SIAM*.

A. Guitton, B. Kaelin and B. Biondi, 2006, Least-square Attenuation of Reverse Time Migration Artifacts, *SEG Exp. Abs.*, 2348–2352.

I. Jones, M.C. Goodwin, I.D. Berranger, H. Zhou and P. Farmer, 2007, Application of anisotropic 3D reverse time migration to complex North Sea imaging, *SEG Exp. Abs.*, 2140–2144.

A.E. Malcolm, B. Ursin and M.V. de Hoop, 2009, Seismic imaging and illumination using multiples *Geophys. J. Intl.*, **176**, 847–864.

D.-J. van Manen, J.O.A. Robertsson and A. Curtis, 2005, Modeling of wave propagation in inhomogeneous media, *Phys. Rev. Lett.*, **94**, 164301.

D.-J. van Manen, A. Curtis and J.O.A. Robertsson, 2006, Interferometric modelling of wave propagation in inhomogeneous elastic media using time-reversal and reciprocity, *Geophysics*, **71**, SI47–SI60.

W. Mulder and A. Ten Kroode, 2002, Automatic velocity analysis by differential semblance optimization *Geophysics*, **67**, 1184–1191.

M. Oristaglio, 1989, An inverse scattering formula that uses all the data *Inverse Problems*, **5**, 1097–1105.

R.-E. Plessix, 2006, A review of the adjoint-state method for computing the gradient of a functional with geophysical applications *Geophys. J. Intl.*, **167**, 495–503.

R.G. Pratt, 1999, Seismic waveform inversion in the frequency domain, part 1: Theory, and verification in a physical scale model *Geophysics*, **64**, 888–901.

R.T. Prosser, 1968, Formal solutions to inverse scattering problems, *J. Math. Phys.*, **10**, 1819–1822.

J.E. Rickett and J.F. Claerbout, 1999, Acoustic daylight imaging via spectral factorization; helioseismology and reservoir monitoring, The Leading Edge, **19**, 957–960.

J.E. Rickett and P.C. Sava, 1999, Offset and angle-domain common image-point gathers for shot-profile migration, *Geophysics*, **67**, 883-889.

J.H. Rose, M. Cheney and B. DeFacio, 1985, Three dimensional inverse scattering: plasma and variable velocity wave equations, *J. Math. Phys.*, **26**, 2803–2813.

P. Sava and B. Biondi, 2004, Wave-equation migration velocity analysis – I: Theory. *Geophys. Prosp.*, **52**,593–606.

P. Sava and I. Vasconcelos, 2010, Extended imaging conditions for wave-equation migration, *Geophys. Prosp.*, *accepted*.

G.T. Schuster, J. Yu, J. Sheng and J. Rickett, 2004, Interferometric/daylight seismic imaging, *Geophys. J. Intl.*, **157**, 838–852.

L. Sirgue and R.G. Pratt, 2004, Efficient waveform inversion and imaging: a strategy for selecting temporal frequencies *Geophysics*, **69**, 231–248.

R.H. Stolt and A.B. Weglein, 1985, Migration and inversion of seismic data, *Geophysics*, **50**, 2458–2472.

W.W. Symes, 2008, Migration velocity analysis and waveform inversion, *Geophys. Prosp.*, **56**, 765–790.

W.W. Symes, 2009, The seismic reflection inverse problem, *Inverse Problems*, **25**, 123008.

C. Tape, Q. Liu, A. Maggi and J. Tromp, 2009, Adjoint tomography of the Southern California crust, *Science*, **325**, 988–992.

A. Tarantola, 1984, Inversion of seismic reflection data in the acoustic approximation, *Geophysics*, **49**, 1259–1256.

J. Thorbecke, 1997, *Common Focus Point Technology*, PhD Thesis, Delft University of Technology.

J. Thorbecke and A.J. Berkhout, 2006, Recursive prestack depth migration using CFP gathers, *Geophysics*, **71**, S273–S283.

J. Thorbecke and K. Wapenaar, 2007, On the relation between seismic interferometry and the migration resolution function, *Geophysics*, **72**, T61–T66.

I. Vasconcelos, 2008, Generalized representations of perturbed fields – applications in seismic interferometry and migration, *SEG Exp. Abs.*, 2927–2941.

I. Vasconcelos and R. Snieder, 2008, Interferometry by deconvolution, Part 1 – Theory for acoustic waves and numerical examples , *Geophysics*, **73**, S115–S128.

I. Vasconcelos, R. Snieder and H. Douma, 2009a, Representation theorems and Greens function retrieval for scattering in acoustic media, *Phys. Rev. E*, **80**, 036605.

I. Vasconcelos, P. Sava and H. Douma, 2009b, Wave-equation extended images via image-domain interferometry, *SEG Exp. Abs.*, 2839–2843.

C.P.A. Wapenaar, G.L. Peels, V. Budejicky and A.J. Berkhout, 1989, Inverse extrapolation of primary seismic waves, Geophysics, **54**, 853–863.

C.P.A. Wapenaar, M.W.P. Dillen and J.T. Fokkema, 2001, Reciprocity theorems for electromagnetic or acoustic one-way wave fields in dissipative inhomogeneous media, Radio Science, **36**, 851–863.

K. Wapenaar, 2004, Retrieving the elastodynamic Green's function of an arbitrary inhomogeneous medium by cross-correlation. *Phys. Rev. Lett.*, **93**, 254301.

K. Wapenaar, J. Thorbecke, and D. Draganov, 2004, Relations between reflection and transmission responses of three-dimensional inhomogeneous media: Geophysical Journal International, **156**, 179–194.

K. Wapenaar, 2006, Green's function retrieval by cross-correlation in case of one-sided illumination: Geophysical Research Letters, **33**, L19304.

K. Wapenaar and J. Fokkema, 2006, Green's function representations for seismic interferometry: Geophysics, **71**, SI33–SI46.

K. Wapenaar, D. Draganov and J. Robertsson, 2006, Introduction to the supplement on seismic interferometry, *Geophysics*, **71**, SI1–SI4.

K. Wapenaar, E. Slob and R. Snieder, 2008, Seismic and electromagnetic controlled-source interferometry in dissipative media, Geophys. Prosp., **56**, 419–434.

K. Wapenaar, 2007, General representations for wavefield modeling and inversion in geophysics: Geophysics, **72**, SM5–SM17.

R.L. Weaver and O.I. Lobkis, 2001, Ultrasonics without a source: Thermal fluctuation correlations and MHz frequencies: Physical Review Letters, **87**, 134301.

A.B. Weglein, F.V. Araújo, P.M. Carvalho, R.H. Stolt, K.H. Matson, R.T. Coates, D. Corrigan, D.J. Foster, S.A. Shaw, and H. Zhang, 2003, Inverse scattering series and seismic exploration: Inverse Problems, **19**, R27–R83

Y. Zhang, S. Xu, N. Bleistein and G. Zhang, 2007, True-amplitude, angle-domain, common-image gathers from one-way wave-equation migrations, *Geophysics*, **72**, S49–S58.